

Full Paper

Synthesis, Cytotoxic Properties and Tubulin Polymerization Inhibitory Activity of Novel 2-Pyrazoline Derivatives

Mohamed Abdel-Aziz¹, Omar M. Aly¹, Sabine S. Khan², Kamalika Mukherjee³, and Susan Bane³¹ Faculty of Pharmacy, Medicinal Chemistry Department, Minia University, Minia, Egypt² SUNY Upstate Medical University, Syracuse, NY, USA³ Biological and Biophysical Chemistry Department, Binghamton University, Binghamton, NY, USA

A series of novel 1-(3',4',5'-trimethoxybenzoyl)-3,5-diarylpyrazoline derivatives were synthesized and evaluated for their cytotoxic properties on different cancer cell lines and tubulin polymerization inhibitory activity. Compounds **6d** and **6e** exhibited remarkable cytotoxic activity against different cancer cell lines with good tubulin polymerization inhibitory activity. Compound **6d** exhibited moderate selectivity toward renal cancer and breast cancer subpanels with selectivity ratios of 3.06 and 5.11, respectively, at the cytostatic activity (TGI) level. Compounds **6e** and **6d** achieved good tubulin polymerization inhibitory activity with IC₅₀ values of 17 and 40 μ M, respectively. The photomicrographs made for compounds **6d** and **6e** on cellular microtubules indicated that the cytotoxicity of these compounds can be attributed to their ability to interfere with microtubule assembly. Molecular modeling studies involving compound **6e** with the colchicine binding site of α , β -tubulin revealed hydrogen-bonding and hydrophobic interactions with several amino acids in the colchicine binding site of β -tubulin.

Keywords: 2-Pyrazoline / Combretastatin A4 / Cytotoxicity / Tubulin polymerization

Received: December 29, 2011; Revised: February 22, 2012; Accepted: February 24, 2012

DOI 10.1002/ardp.201100471

Introduction

Cancer is a major cause of death around the world. The WHO projected 12 million deaths by cancer with existing therapeutics by 2030. Out of the 27 types of characterized cancers, only lung, stomach, liver, colon, and breast cancers are mainly implicated in cancer mortality. Taking into consideration the existing cancer therapies, chemotherapy has turned out to be one of the most significant treatments in cancer management [1]. Moreover, cancer chemotherapy has entered a new era of molecularly targeted therapeutics, which is highly selective and not associated with the serious toxicities of conventional cytotoxic drugs [2]. The combretastatins are a group of antimetabolic agents isolated from the bark of the South African tree *Combretum caffrum* [3]. The most active of these, combretastatin A4 (CA4) (**I**), is a potent cytotoxic agent that strongly inhibits the polymerization of tubu-

lin by binding to the colchicine-binding site of the β -tubulin subunit [4]. Tubulin therefore remains an important target for the design of anticancer agents. Interference with tubulin/microtubule polymerization dynamics has two key anticancer effects: (i) inhibition of cancer cell proliferation through disturbance of mitotic spindle function, which leads to cell apoptosis [5], and (ii) disruption of cell signaling pathways involved in regulating and maintaining the cytoskeleton of endothelial cells in tumor vasculature. It must be emphasized that the therapeutic effects of these agents such as CA4 are derived from their vasculature targeting properties and not antimetabolic properties. Because of its structural simplicity, a wide number of CA4 analogues have been developed and assessed as potential anticancer agents, some of which have recently been reviewed [6–16]. Further interest in combretastatin derivatives was stimulated by the discovery that CA4 is also able to elicit irreversible vascular shutdown within solid tumors, leaving normal vasculature intact [17, 18]. In this way tumors are starved of oxygen and nutrients and their constituent cells die. Agents that act in this manner have the potential to make a significant impact on the clinical management of cancer [19]. A prodrug of combreta-

Correspondence: Mohamed Abdel-Aziz, Faculty of Pharmacy, Medicinal Chemistry Department, Minia University, Minia 61519, Egypt.

E-mail: abulnil@hotmail.com**Fax:** +2086 2369075

statin A4, the water-soluble phosphate derivative Zybrestat is now in phase III clinical trials for the treatment of cancer [20]. Many analogs of CA4 have been designed to study the structure-activity relationship of the molecule in order to enhance both the cytotoxic and selective vascular targeting activity [21–32]. Among synthetic small molecule tubulin inhibitors, replacement of the olefinic bridge of **I** with a carbonyl group furnished a benzophenone-type CA4 analogue named phenstatin (**IIa**). This compound demonstrated interesting efficacy in a variety of tumor models, while retaining the characteristics of **I** [33]. The 2-aminobenzophenone derivative (**IIb**) also strongly inhibited cancer cell growth and tubulin polymerization and caused mitotic arrest, the same as in compound **IIa** [34]. A series of methoxy substituted 2-(3',4',5'-trimethoxybenzoyl)benzo[b]furan [35], -benzo[b]thiophene (**IIIa** and **IIIb**) [36–38] (Chart 1), and indole [39] derivatives were found to inhibit the growth of different cancer cell lines and tubulin polymerization by binding to the colchicine site of tubulin and caused G2-M phase arrest of the cell cycle. In addition, pyrazole derivatives are well established in the literature as important biologically effective heterocyclic compounds. These derivatives are the subject of many research studies due to their widespread potential pharmacological activities such as anti-inflammatory [40], antipyretic [41], antimicrobial [42], antiviral [43], antitumor [44], anticonvulsant [45], antihistaminic [46], and antidepressant [47] activities. Promoted with the above-mentioned studies and as a continuation of our research interest in the synthesis and biological activities of novel pyrazole derivatives [48–50], and in order to further investigate structural determinants of cytotoxic activity of this class of compounds, the present work involves a flexible, concise, and highly convergent protocol for the synthesis of novel series of 1-(3',4',5'-trimethoxybenzoyl)-3,5-diaryl-2-pyrazoline derivatives having variously substituted 3- and 5-aryl rings aimed to investigate the effect of introducing additional aryl unit, keeping in mind the presence of 3',4',5'-trimethoxyphenyl of the 2-benzoyl moiety unchanged because it is the characteristic structural requirement for

activity in a numerous inhibitors of tubulin polymerization, such as colchicine, CA4, and podophyllotoxin [51–54]. The prepared pyrazoline derivatives that carry three different aryl groups were evaluated for both *in vitro* cytotoxic properties on different cancer cell lines and tubulin polymerization inhibitory activity. Furthermore, molecular modeling studies of the most active tubulin inhibitor with the colchicine binding site of α,β -tubulin was also performed.

Results and discussion

Chemistry

Chalcones (**3a–g**, Scheme 1) were synthesized by a base catalyzed Claisen-Schmidt condensation reaction of appropriately substituted acetophenones (**1a–b**) and substituted aromatic aldehydes (**2a–f**) in the presence of 10% NaOH in ethanol. Heating at reflux chalcones (**3a–g**) with hydrazine monohydrate 95% in absolute ethanol afforded the corresponding pyrazolines (**4a–g**). ^1H NMR spectra recorded for the prepared compounds clearly supported the proposed structures, protons of pyrazoline ring in compounds **4a**, **4c**, **4d**, **4e**, **4f**, and **4g** showed a prominent ABX system, with protons Ha, Hb, and Hx seen as doublets of doublets at δ 2.96–3.30, 3.40–3.54, and 4.82–5.27 ppm ($J_{\text{Ha-Hb}} = 16.30$ – 16.86 Hz, $J_{\text{Ha-Hx}} = 7.33$ – 9.34 Hz, and $J_{\text{Hb-Hx}} = 9.90$ – 10.62 Hz), respectively. On the other hand, pyrazoline **4b** with substituted benzaldehyde carrying highly electronegative groups (2,6-dichloro) made Ha and Hb that appeared to be equivalent, so the pattern became AX system. The CH_2 protons appeared as doublet at δ 3.46 ppm while the CH proton appeared as triplet at δ 5.80 ppm ($J = 11.90$ Hz). The protons belonging to the aromatic system and phenyl substituents were observed at the expected chemical shifts and integral values. Coupling of pyrazolines (**4a–g**) with 3,4,5-trimethoxybenzoyl chloride **5** in CH_2Cl_2 in the presence of triethylamine afforded the formation of the corresponding 1-(3',4',5'-trimethoxybenzoyl)-3,5-diarylpyrazoline derivatives **6a–g** (Scheme 1). The structure of the prepared compounds was

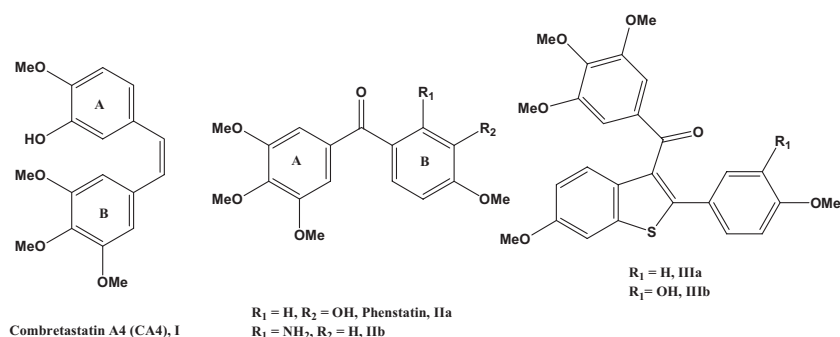
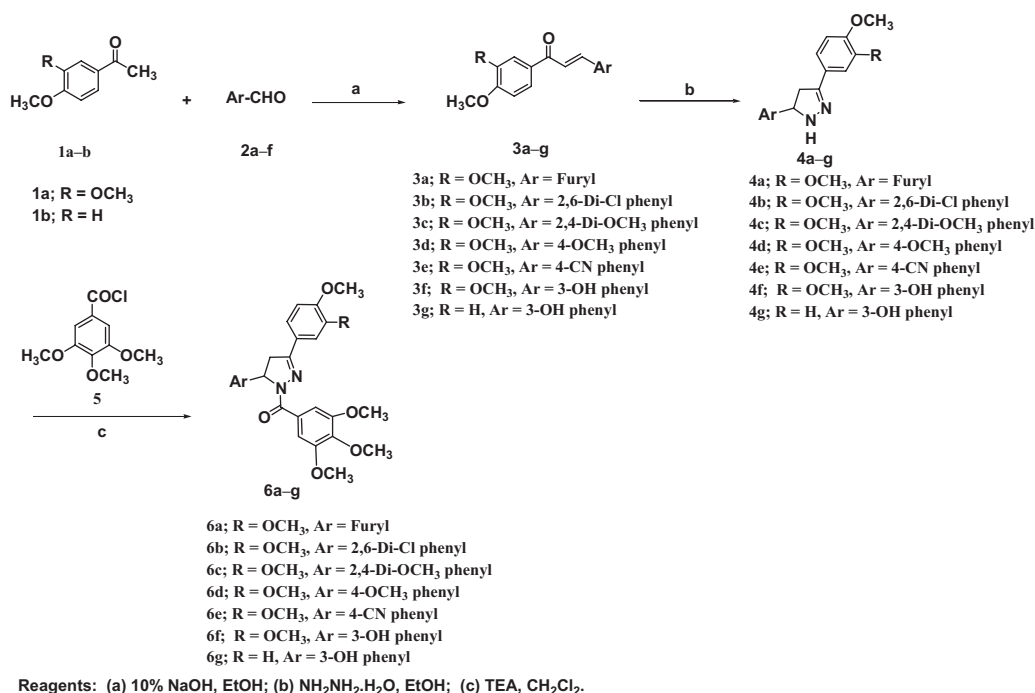


Chart 1. Different inhibitors for tubulin polymerization.



Scheme 1. Synthesis of novel pyrazoline derivatives **6a–g**.

confirmed by the appearance of an additional strong absorption band of (C=O) stretching at $1570\text{--}1585 \text{ cm}^{-1}$ and disappearance of that of NH stretching in IR spectra. The $^1\text{H NMR}$ spectra showed additional peaks each for the CH_3 protons in addition to the protons of the phenyl moiety at the expected aromatic region. The structure of the prepared compounds was confirmed on the basis of their IR, $^1\text{H NMR}$, $^{13}\text{C NMR}$, mass spectra, and elemental analysis.

Biological investigations

Screening of anticancer activity

Compounds **6b**, **6c**, **6d**, and **6e** were selected by the National Cancer Institute (NCI) according to the protocol of the Drug Evaluation Branch of the National Cancer Institute, Bethesda, USA for *in vitro* anticancer screening. Primary *in vitro* one dose anticancer assay was performed in full NCI 60 cell lines derived from nine tumor subpanels, including leukemia, melanoma, lung, colon, CNS, ovarian, renal, prostate, and breast cancer cell lines. The selected compounds were added at a single concentration (10^{-5} M) and the culture was incubated for 48 h. End point determinations were made with a protein binding dye sulforhodamine B (SRB). Results for each compound were reported as a mean graph of the percent growth of the treated cells when compared to the untreated control cells.

The pyrazoline derivative **6d** achieved remarkable cell growth inhibition activity against most of the tested cell lines and the results were illustrated in Table 1.

The results in Table 2 indicate that the pyrazoline derivative **6e** exhibited broad spectrum of cell growth inhibition activity against most of the tested cell lines.

Pyrazoline derivative **6b** exhibited moderate cell growth inhibition activity against leukemia SR, melanoma SK-MEL-5, and renal cancer UO-31 cell lines. Compound **6c** also exhibited broad-spectrum cell growth inhibition activity against melanoma MDA-MB-435, renal cancer CAKI-1, and breast cancer MCF7 cell lines. Pyrazoline derivative **6c** revealed moderate cell growth inhibition against melanoma SK-MEL-5 and renal cancer UO-31 cell lines.

The obtained results indicate that the pyrazoline derivatives **6d** and **6e** exhibited the highest ability to inhibit the proliferation of different cancer cell lines (Tables 1 and 2) compared to pyrazoline derivatives **6b** and **6c**. A different aldehyde substituent used in the position 5 of the synthesized pyrazoline derivative might contribute to the activity of the synthesized compounds; the presence of only one OCH_3 group is preferable over the presence of two OCH_3 groups (pyrazoline **6d** has better anticancer activity against different cancer cell lines, better than pyrazoline **6c**). Also the presence of an electron withdrawing group (CN) in pyrazoline **6e** has better anticancer activity against different cancer cell lines.

In vitro five dose full NCI 60 cell panel assay

The pyrazoline derivatives **6d** and **6e** were selected for advanced five dose testing against the full panel of 60 human

Table 1. One dose mean graph of nine different cancer cell types of compound **6d**

Panel	Cell line	Growth percent	Panel	Cell line	Growth percent
Leukemia	CCRF-CEM	24.31	Ovarian cancer	IGROV1	31.49
	HL-60(TB)	5.49		OVCAR-3	−45.13
	K-562	28.31		OVCAR-4	58.83
	MOLT-4	47.08		OVCAR-5	66.53
	RPMI-8226	50.20		OVCAR-8	34.16
Non-small cell lung cancer	SR	20.62	NCI/ADR-RES	12.99	
	A549/ATCC	27.23	SK-OV-3	30.31	
	EKVX	48.16	786-0	26.74	
	HOP-62	34.76	ACHN	48.71	
	NCI-H226	51.94	CAKI-1	12.09	
	NCI-H23	46.60	RXF-393	−21.41	
	NCI-H322M	37.72	SN12C	41.49	
Colon cancer	NCI-H460	6.07	TK-10	18.39	
	NCI-H522	−35.93	UO-31	21.07	
	COLO 205	8.03	PC-3	30.53	
	HCC-2998	61.11	DU-145	11.62	
	HCT-116	20.59	MCF7	27.60	
	HCT-15	32.84	MDA-MB-231/ATCC	12.55	
	HT29	−1.10	HS 578T	−14.04	
CNS cancer	KM12	16.15	BT-549	27.57	
	SW-620	20.86	T-47D	36.39	
	SF-268	54.74	MDA-MB-468	−32.54	
	SF-295	4.28			
	SF-539	−14.46			
Melanoma	SNB-19	38.90			
	U251	26.05			
	LOX IMVI	36.06			
	MALME-3M	57.74			
	M14	−11.78			
	MDA-MB-435	−26.63			
	SK-MEL-2	12.61			
	SK-MEL-28	70.51			
	SK-MEL-5	5.80			
	UACC-257	66.30			
UACC-62	41.88				

tumor cell lines. All the 60 cell lines representing nine tumor subpanels were incubated at five different concentrations (0.01, 0.1, 1, 10, and 100 μM). The outcomes were used to create log concentration versus % growth inhibition curves and three response parameters (GI_{50} , TGI, and LC_{50}) were calculated for each cell line. The GI_{50} value (growth inhibitory activity) corresponds to the concentration of the compound causing 50% decrease in net cell growth, the TGI value (cytostatic activity) is the concentration of the compound resulting in total growth inhibition (TGI) and LC_{50} value (cytotoxic activity) is the concentration of the compound causing net 50% loss of initial cells at the end of the incubation period of 48 h. Compound **6d** exhibited remarkable anticancer activity against most of the tested cell lines representing nine different subpanels. Compound **6d** showed high activity against most of the tested cell lines with GI_{50} ranging from 0.19 to $>100 \mu\text{M}$ (Table 3). The criterion for selectivity of a compound depends upon the ratio obtained by dividing the full panel MID (the average sensi-

tivity of all cell lines toward the test agent) (μM) by their individual subpanel MID (μM). Ratios between 3 and 6 refer to moderate selectivity; ratios >6 indicate high selectivity toward the corresponding cell line, while compounds not meeting either of these criteria rated non-selective [55]. In this context, compound **6d** was found to have broad-spectrum antitumor activity against the nine tumor subpanels tested with selectivity ratios ranging between 0.52 and 5.11 at the GI_{50} level. Compound **6d** exhibited moderate selectivity toward the renal cancer subpanel with selectivity ratio of 3.06 at GI_{50} level and toward the breast cancer subpanel with selectivity ratio of 5.11 at GI_{50} level.

Compound **6e** exhibited remarkable anticancer activity against most of the tested cell lines representing nine different subpanels with GI_{50} values between 0.19 and $12.7 \mu\text{M}$ (Table 4).

The criterion for selectivity of compound **6e** was found to be broad-spectrum antitumor activity against the nine tumor

Table 2. One dose mean graph of nine different cancer cell types of compound **6e**

Panel	Cell line	Growth percent	Panel	Cell line	Growth percent
Leukemia	CCRF-CEM	29.95	Ovarian cancer	IGROV1	13.42
	HL-60(TB)	4.24		OVCAR-3	-47.81
	K-562	20.64		OVCAR-4	62.13
	MOLT-4	49.49		OVCAR-5	58.79
	RPMI-8226	60.79		OVCAR-8	32.83
Non-small cell lung cancer	SR	28.45	NCI/ADR-RES	2.92	
	A549/ATCC	22.03	SK-OV-3	19.78	
	EKVX	33.40	Renal cancer	786-0	25.13
	HOP-62	36.09		ACHN	44.56
	NCI-H226	52.41		CAKI-1	5.45
	NCI-H23	43.19		RXF-393	-17.21
	NCI-H322M	36.95	SN12C	53.55	
NCI-H460	9.81	TK-10	31.92		
NCI-H522	-15.98	UO-31	18.21		
Colon cancer	COLO 205	-9.28	Prostate cancer	PC-3	31.38
	HCC-2998	35.19		DU-145	5.75
	HCT-116	13.56	Breast cancer	MCF7	26.96
	HCT-15	26.67		MDA-MB-231/ATCC	18.22
	HT29	-8.40		HS 578T	-18.29
	KM12	15.12		BT-549	28.63
	SW-620	16.09		T-47D	37.14
CNS cancer	SF-268	49.33	MDA-MB-468	-25.76	
	SF-295	-3.96			
	SF-539	-13.27			
	U251	21.54			
Melanoma	LOX IMVI	33.58			
	MALME-3M	39.46			
	M14	-6.86			
	MDA-MB-435	-40.37			
	SK-MEL-2	35.64			
	SK-MEL-28	65.29			
	SK-MEL-5	17.74			
	UACC-257	69.25			
UACC-62	43.60				

subpanels tested with selectivity ratios ranging between 0.70 and 1.69 at the GI_{50} level. Compound **6e** exhibited no selectivity toward the tested cell lines.

Tubulin polymerization inhibitory assay

To investigate whether the cytotoxicity of the synthesized pyrazoline derivatives were related to the interaction with tubulin, pyrazolines **6c**, **6d**, **6e**, and **6f** were tested *in vitro* for tubulin polymerization inhibitory activity (Fig. 1 and Table 5). Inhibition of paclitaxel-induced tubulin polymerization was determined by monitoring DAPI fluorescence as previously described [56, 57]. Bonne et al. [57] demonstrated that the DNA-binding dye, 4',6-diamidino-2-phenylindole (DAPI), binds to tubulin at a site distinct from the three major drug-binding sites, resulting in enhanced DAPI fluorescence. The affinity of DAPI for assembled tubulin is greater than its affinity for unpolymerized tubulin, so tubulin assembly

produces a net increase in the emission intensity of DAPI. The use of the fluorescence method has the following advantages: rapid, easy to perform, with good accuracy and reproducibility, lower sample volumes, and concentrations can be used in fluorescence spectroscopy. The solubility of the tested compounds was first determined in the assay conditions specified under experimental procedures. It was found that each drug approached its solubility limit at 40 μ M concentration in 2% DMSO. The drugs (40 μ M) were then screened for their potential ability to inhibit microtubule formation. In the polymerization experiments; a fixed concentration of protein (5 μ M) was induced to polymerize in the presence of a fixed concentration of drug (40 μ M). If a test drug is strongly cytotoxic and the effect is mediated through microtubules, then we expect to see it affect tubulin assembly under these conditions. If it does not, then a non-microtubule mechanism for cytotoxicity is more likely.

Table 3. NCI *in vitro* testing results of compound **6d** at five dose level in μM

Panel	Cell line	GI ₅₀			TGI	LC ₅₀
		Conc. per cell line	Subpanel MID ^b	Selectivity ratio (MID ^a /MID ^b)	Conc. per cell line	
Leukemia	CCRF-CEM	4.29	5.23	1.34	>100	>100
	HL-60(TB)	3.80			>100	>100
	K-562	1.78			>100	>100
	MOLT-4	11.10			>100	>100
	RPMI-8226	4.27			>100	>100
Non-small cell lung cancer	SR	6.16	13.35	0.52	>100	>100
	A549/ATCC	2.88			>100	>100
	EKVX	7.60			>100	>100
	HOP-62	1.67			>100	>100
	HOP-92	0.19			0.93	>100
	NCI-H226	0.59			>100	>100
	NCI-H23	3.08			>100	>100
	NCI-H322M	>100			>100	>100
	NCI-H460	3.71			>100	>100
	NCI-H522	0.46			>100	>100
Colon cancer	COLO 205	2.50	2.51	2.79	7.86	>100
	HCC-2998	1.85			4.77	>100
	HCT-116	2.48			>100	>100
	HCT-15	1.32			>100	>100
	HT29	3.11			>100	>100
	KM12	2.18			39.80	>100
	SW-620	4.11			>100	>100
CNS cancer	SF-268	5.61	2.56	2.73	>100	>100
	SF-295	0.68			>100	>100
	SF-539	1.15			4.71	>100
	SNB-19	3.82			>100	>100
	SNB-75	1.61			>100	>100
	U251	2.48			>100	>100
Melanoma	LOX IMVI	2.55	19.45	0.36	>100	>100
	MALME-3M	83.40			>100	>100
	M14	2.40			>100	>100
	MDA-MB-435	0.45			2.30	>100
	SK-MEL-2	3.05			>100	>100
	SK-MEL-28	72.2			>100	>100
	SK-MEL-5	0.32			3.21	>100
	UACC-257	9.92			>100	>100
	UACC-62	0.75			>100	>100
	Ovarian cancer	IGROV1			4.76	3.85
OVCAR-3		0.98	2.91	>100		
OVCAR-4		5.66	>100	>100		
OVCAR-5		9.27	>100	>100		
OVCAR-8		3.62	>100	>100		
NCI/ADR-RES		1.04	7.85	>100		
Renal cancer	SK-OV-3	1.64	2.29	3.06	>100	>100
	786-0	3.95			>100	>100
	A498	0.54			nd	>100
	ACHN	1.06			>100	>100
	CAKI-1	0.66			>100	>100
	RXF-393	0.34			3.05	>100
	SN12C	5.90			>100	>100
	TK-10	4.87			>100	>100
	UO-31	1.03			>100	>100
Prostate cancer	PC-3	2.86	2.43	2.88	>100	>100
	DU-145	4.01			>100	>100

Table 3. (continued)

Panel	Cell line	GI ₅₀			TGI	LC ₅₀
		Conc. per cell line	Subpanel MID ^b	Selectivity ratio (MID ^a /MID ^b)	Conc. per cell line	
Breast cancer	MCF7	0.63	1.37	5.11	>100	>100
	MDA-MB-231/ATCC	2.84			>100	>100
	HS 578T	1.55			>100	>100
	BT-549	2.28			21.8	>100
	T-47D	0.61			>100	>100
	MDA-MB-468	0.33	4.66	>100		
MID ^a			7.00			

MID^a = Average sensitivity of all cell lines in μM .

MID^b = Average sensitivity of all cell lines of a particular subpanel in μM .

nd, Not determined.

Table 4. NCI *in vitro* testing results of compound 6e at five dose level in μM .

Panel	Cell line	GI ₅₀			TGI	LC ₅₀		
		Conc. per cell line	Subpanel MID ^b	Selectivity ratio (MID ^a /MID ^b)	Conc. per cell line			
Leukemia	CCRF-CEM	3.53	2.83	0.70	>100	>100		
	HL-60(TB)	1.89			5.62	>100		
	K-562	1.30			>100	>100		
	MOLT-4	4.43			>100	>100		
	RPMI-8226	3.53			>100	>100		
	SR	2.28			>100	>100		
Non-small cell lung cancer	A549/ATCC	2.32	2.53	0.78	>100	>100		
	EKVX	4.57			>100	>100		
	HOP-62	1.53			36.90	>100		
	HOP-92	0.19			0.99	>100		
	NCI-H226	0.75			30.6	>100		
	NCI-H23	2.93			54.8	>100		
	NCI-H322M	7.97			85.3	>100		
	NCI-H460	2.34			>100	>100		
	NCI-H522	0.18			0.49	4.81		
	COLO 205	1.47			1.58	4.03	>100	
Colon cancer	HCC-2998	2.16	1.58	1.25	6.63	>100		
	HCT-116	1.76			19.5	>100		
	HCT-15	1.10			42.1	>100		
	HT29	2.13			10.3	95.20		
	KM12	1.03			7.44	>100		
	SW-620	1.44			>100	>100		
	SF-268	2.48			1.16	1.69	44.40	>100
	SF-295	0.40			7.23	69.90		
CNS cancer	SF-539	0.58	1.16	1.69	3.35	>100		
	SNB-19	1.75			46.50	>100		
	SNB-75	0.55			11.00	>100		
	U251	1.21			11.90	78.90		
	LOX IMVI	2.37			2.38	0.83	15.00	>100
	MALME-3M	12.7			62.20	>100		
Melanoma	M14	2.03	2.38	0.83	12.40	>100		
	MDA-MB-435	0.34			1.01	39.60		
	SK-MEL-2	0.71			4.12	48.90		
	SK-MEL-28	1.80			30.20	>100		
	SK-MEL-5	0.39			5.65	>100		
	UACC-257	0.70			28.30	>100		
	UACC-62	0.40			28.20	>100		

continued

Table 4. (continued)

Panel	Cell line	GI ₅₀			TGI	LC ₅₀
		Conc. per cell line	Subpanel MID ^b	Selectivity ratio (MID ^a /MID ^b)	Conc. per cell line	
Ovarian cancer	IGROV1	1.87	1.87	1.05	23.40	>100
	OVCAR-3	0.42			1.70	7.03
	OVCAR-4	2.09			42.40	>100
	OVCAR-5	4.21			>100	>100
	OVCAR-8	2.87			18.20	>100
	NCI/ADR-RES	0.75			41.50	>100
Renal cancer	SK-OV-3	0.89	1.53	1.29	7.05	>100
	786-0	2.62			23.80	>100
	A498	0.37			4.34	>100
	ACHN	0.65			44.20	>100
	CAKI-1	0.43			25.40	>100
	RXF-393	0.42			3.03	48.00
	SN12C	3.96			>100	>100
	TK-10	3.32			20.30	>100
Prostate cancer	UO-31	0.46	2.71	0.73	17.80	>100
	PC-3	1.89			27.40	>100
	DU-145	3.53			15.20	>100
Breast cancer	MCF7	0.48	1.39	1.42	79.00	>100
	MDA-MB-231/ATCC	2.27			20.80	>100
	HS 578T	0.99			6.74	>100
	BT-549	2.09			11.00	>100
	T-47D	2.21			95.30	>100
	MDA-MB-468	0.30			1.92	>100
MID ^a				1.97		

MID^a = Average sensitivity of all cell lines in μM .

MID^b = Average sensitivity of all cell lines of a particular subpanel in μM .

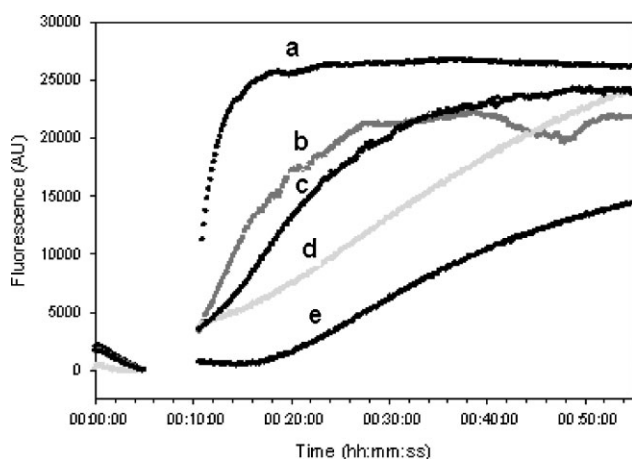


Figure 1. Effect of compounds **6c–f** on paclitaxel-induced tubulin assembly. Bovine brain tubulin ($5 \mu\text{M}$) in PME buffer; and 0.1 mM GTP was incubated with $40 \mu\text{M}$ of various tested compounds for 40 min at room temperature. Microtubule assembly was then induced by paclitaxel ($5 \mu\text{M}$) at 37°C . The final concentration of DMSO in each sample was $2\% \text{ v/v}$. Polymerization was monitored by the change in fluorescence of microtubule-bound DAPI at excitation and emission wavelengths of 360 and 450 nm, respectively. The curves shown are the control with no ligand (a), and samples containing $40 \mu\text{M}$ of the tested drug; **6c** (c), **6d** (b), **6e** (e), and **6f** (d).

Table 5. Inhibition of tubulin assembly induced by compounds **6c–f** ($40 \mu\text{M}$)

Compound	Percent inhibition ^{a)}
6c	11
6d	15
6e	40
6f	11

^{a)} Decrease in assembly relative to a control without added drug. Data were collected as described in Fig. 1.

Figure 1 shows a typical polymerization profile. The relative potencies of each compound are expressed as the decrease in the fluorescence signal at the plateau relative to the control (Table 5).

These results indicate that there is a positive correlation between tubulin polymerization and cytotoxic activity of the tested pyrazoline derivatives. The results indicate that pyrazolines **6e** and **6d** which exhibited good cytotoxic activity against different cancer cell lines achieved also good tubulin polymerization inhibitory activity. Compound **6d** exhibited moderate selectivity toward renal cancer subpanel with selec-

ligand) were uninucleated and exhibited a dense network of microtubules whereas the cells treated with 20 μM of compound **6d** or **6e** were multinucleated (indicated by an arrow) and showed a diffused microtubule network. The photomicrographs thus indicate that the cytotoxicity of these drugs can be attributed to their ability to interfere with microtubule assembly.

Molecular modeling

Molecular docking studies of pyrazoline **6e** to tubulin protein were performed. The X-ray crystal structure of the DAMA-colchicine-tubulin complex (PDB code 1SA0) was used as the tubulin protein template. As shown in Fig. 3 (*S*-isomer of compound **6e**), the pyrazoline bridge moiety of compound **6e** causes the ring-A and ring-B to lie in similar positions to that of the colchicine. In the ring-A (trimethoxyphenyl) of compound **6e**, the $-\text{OCH}_3$ substituted on it can form hydrogen bonds with Cys241 in β -subunit (3.63, 4.16, or 4.92 Å). The ring-B of compound **6e** (dimethoxyphenyl) the *p*- OCH_3 on it can support hydrogen bond interactions with the backbone at Val315 or Lys352 in β -subunit (distances 2.15 or 2.89 Å, respectively). The CN group can accept a hydrogen bond with the Glu183 (distance 3.97 Å). Hydrophobic interactions were also observed between different methyl groups of compound **6e** with different amino acids including Val181, Leu248, and Leu255 in the colchicine binding site of β -tubulin.

Conclusions

A group of novel 2-pyrazoline derivatives was prepared as combretastatin A4 analogues and characterized by different spectroscopic and elemental analysis techniques. The prepared pyrazoline derivatives were evaluated for both anticancer activity on different cancer cells and tubulin polymerization inhibitory activity. The results revealed that pyrazoline derivatives **6d** and **6e** exhibited remarkable cytotoxic activity against different cancer cell lines. The results indicate that there is a positive correlation between tubulin polymerization inhibitory activity and cytotoxicity of the tested pyrazolines **6d** and **6e**. Compound **6d** exhibited moderate selectivity toward the renal cancer subpanel with selectivity ratio of 3.06 at GI_{50} level and toward the breast cancer subpanel with selectivity ratio of 5.11 at GI_{50} level. The IC_{50} value was calculated for compounds **6e** and **6d** and was found to be 17 and 40 μM , respectively. The photomicrographs made for compounds **6d** and **6e** on cellular microtubules indicate that the cytotoxicity of these compounds is attributed to their ability to interfere with microtubule assembly. Molecular modeling studies involving compound **6e** with the colchicine binding site of α,β -tubulin revealed hydrogen-bonding and hydrophobic interactions with several

amino acids in the colchicine binding site of β -tubulin. Finally, the novel synthesized pyrazoline derivatives **6d** and **6e** are promising anticancer agents and tubulin polymerization inhibitory activity may be the expected mechanism of action of these compounds.

Experimental

Chemistry

Melting points were determined on Stuart electrothermal melting point apparatus and were uncorrected. IR spectra were recorded as KBr disks on a Bruker Vector 22 IR spectrophotometer. NMR spectra were carried out on 300 MHz Mercury 300BB NMR spectrophotometer and a Bruker Advance 300 MHz NMR spectrometer, using TMS as internal reference. Chemical shifts (δ values are given in parts per million (ppm) relative to CDCl_3 (7.29 for proton and 76.9 for carbon) or $\text{DMSO}-d_6$ (2.50 for proton and 39.50 for carbon) and coupling constants (*J*) in Hertz. Splitting patterns are designated as follows: s, singlet; d, doublet; t, triplet; q, quartet; dd, doublet of doublet; m, multiplet. Accurate masses were obtained on a Micromass LCT mass spectrometer and on an Agilent Technologies 1100 LC/MSD ion trap mass spectrometer equipped with an atmospheric pressure electrospray. The progress of reactions and the purity of the prepared compounds were monitored by thin-layer chromatography (TLC) using Merck 9385 pre-coated aluminum plate silica gel (Kieselgel 60) 5 cm \times 20 cm plates with a layer thickness of 0.2 mm. The spots were detected by exposure to UV-lamp at $\lambda = 254$ nm. Elemental analysis was performed on a Perkin Elmer 2400 CHN elemental analyzer, and the results were within $\pm 0.4\%$ of the theoretical values.

Chalcones (**3a–g**) were prepared according to reported procedure [59].

Compounds (**4a–g**) were prepared according to reported procedure [48].

5-(3-Hydroxyphenyl)-4,5-dihydro-3-(4-methoxyphenyl)-1H-pyrazole (**4g**)

Yellowish white crystals (ethanol) in (2.00 g, 74.63% yield), mp 179–180°C. IR (KBr) ν_{max} (cm^{-1}): 3410 (OH), 3322 (NH), 1592 (C=N), and 1575 (C-C). ^1H NMR (300 MHz, CDCl_3) δ (ppm): 3.15 (dd, 1H, *J* = 16.76 and 7.40 Hz, CH_2 of pyrazoline), 3.44 (dd, 1H, *J* = 16.76 and 10.30 Hz, CH_2 of pyrazoline), 3.70 (s, 3H, OCH_3), 4.82 (dd, 1H, *J* = 7.40 and 10.30 Hz, CH of pyrazoline), 6.41–6.68 (m, 5H, Ar-H), 6.94 (dd, 2H, *J* = 8.10 and 2.10 Hz, Ar-H), 7.17 (s, 1H, NH), 7.25 (d, 1H, *J* = 1.83 Hz, Ar-H). MS: *m/z* (%) 269 (100) [$\text{M}+1$], 268 (100) [M^+], 267 (68), 155 (60). Anal. Calcd. for $\text{C}_{16}\text{H}_{16}\text{N}_2\text{O}_2$: C, 71.62; H, 6.01; N, 10.44. Found: C, 71.73; H, 6.08; N, 10.44.

General procedure for preparation of compounds (**6a–g**)

To a stirred solution of pyrazoline derivatives **4a–f** (1.0 mmol) in 20 mL CH_2Cl_2 was added compound **5** (0.63 g; 2.0 mmol) followed by triethylamine (0.22 g; 2.2 mmol). The mixture was stirred for 1 h at room temperature; the reaction was quenched by the addition of 20 mL saturated NaCl and 20 mL EtOAc. The aqueous layer was extracted with (2 \times 20 mL) EtOAc, the combined EtOAc extracts were washed subsequently with 10 mL 1 N HCl (2 \times 10 mL) distilled H_2O , 10 mL NaHCO_3 (2 \times 10 mL)

distilled H₂O and 10 mL saturated NaCl, and dried over MgSO₄. After complete evaporation of the organic solvents using a vacuum pump the crude product was purified by silica gel column chromatography using ethyl acetate/*n*-hexane as a mobile phase to give compounds **6a–g**.

5-(2-Furyl)-4,5-dihydro-1-(3,4,5-trimethoxybenzoyl)-3-(3,4-dimethoxyphenyl)-1H-pyrazole (6a)

The residue was chromatographed with ethyl acetate/*n*-hexane (1:4) as eluent to give **6a** as a white powder in (0.39 g, 83.69% yield), mp 180°C. IR (KBr) ν_{\max} (cm⁻¹): 1615 (C=N), 1578 (C=O). ¹H NMR (300 MHz, CDCl₃) δ (ppm): 3.50 (dd, 1H, *J* = 17.40 and 5.10 Hz, CH₂ of pyrazoline), 3.65 (dd, 1H, *J* = 17.40 and 11.40 Hz, CH₂ of pyrazoline), 3.92 (s, 3H, CH₃), 3.94 (s, 9H, 3CH₃), 3.96 (s, 3H, CH₃), 5.94 (dd, 1H, *J* = 5.10 and 11.40 Hz, CH of pyrazoline), 6.35–6.37 (m, 1H, Ar-H), 6.44 (d, 1H, *J* = 3.30 Hz, Ar-H), 6.91 (d, 1H, *J* = 8.10 Hz, Ar-H), 7.22 (dd, 1H, *J* = 8.10 and 1.80 Hz, Ar-H), 7.35 (s, 1H, Ar-H), 7.41 (d, 1H, *J* = 1.80 Hz, Ar-H), 7.47 (s, 2H, Ar-H). ¹³C NMR (75 MHz, CDCl₃) δ (ppm): 39.53 (CH₂), 57.03 (CH₃), 57.86 (CH₃), 58.01 (CH₃), 58.18 (2CH₃), 62.84 (CH), 109.24 (CH), 109.50 (CH), 109.90 (CH), 111.94 (CH), 112.09 (CH), 121.91 (CH), 125.32 (CH), 129.98 (C), 141.59 (C), 142.93 (C), 150.09 (C), 152.18 (C), 152.89 (C), 153.11 (C), 155.57 (C), 165.80 (CO). MS (ESI): 467.3 (C₂₅H₂₇N₂O₇, [M+H]⁺). Anal. Calcd. for C₂₅H₂₆N₂O₇: C, 64.37; H, 5.62; N, 6.01. Found: C, 64.14; H, 5.66; N, 5.97.

5-(2,6-Dichlorophenyl)-4,5-dihydro-1-(3,4,5-trimethoxybenzoyl)-3-(3,4-dimethoxyphenyl)-1H-pyrazole (6b)

The residue was chromatographed with ethyl acetate/*n*-hexane (1:3) as eluent to give **6b** as a white solid in (0.44 g, 80.73% yield), mp 191–192°C. IR (KBr) ν_{\max} (cm⁻¹): 1608 (C=N), 1580 (C=O). ¹H NMR (300 MHz, CDCl₃) δ (ppm): 3.41 (dd, 1H, *J* = 17.40 and 8.70 Hz, CH₂ of pyrazoline), 3.77 (dd, 1H, *J* = 17.40 and 12.60 Hz, CH₂ of pyrazoline), 3.92 (s, 3H, CH₃), 3.93 (s, 3H, CH₃), 3.94 (s, 6H, 2CH₃), 3.96 (s, 3H, CH₃), 6.48 (dd, 1H, *J* = 8.70 and 12.60 Hz, CH of pyrazoline), 6.92 (d, 1H, *J* = 8.40 Hz, Ar-H), 7.16 (d, 1H, *J* = 7.80 Hz, Ar-H), 7.21 (d, 1H, *J* = 8.4 Hz, Ar-H), 7.29 (d, 1H, *J* = 7.80 Hz, Ar-H), 7.40 (s, 1H, Ar-H), 7.42 (d, 1H, *J* = 1.80 Hz, Ar-H), 7.46 (s, 2H, Ar-H). ¹³C NMR (75 MHz, CDCl₃) δ (ppm): 40.23 (CH₂), 57.88 (CH₃), 58.02 (CH₃), 58.15 (2CH₃), 60.03 (CH₃), 62.83 (CH), 109.58 (CH), 109.93 (CH), 112.14 (CH), 121.73 (CH), 125.29 (CH), 129.69 (CH), 129.74 (CH), 130.19 (C), 131.07 (C), 134.79 (C), 135.97 (C), 137.23 (C), 141.62 (C), 150.12 (C), 152.12 (C), 153.10 (C), 155.15 (C), 165.84 (CO). MS (ESI): 545.2 (C₂₇H₂₇Cl₂N₂O₆, [M+H]⁺). Anal. Calcd. for C₂₇H₂₆Cl₂N₂O₆: C, 59.46; H, 4.80; N, 5.14. Found: C, 59.43; H, 5.04; N, 5.15.

1-(3,4,5-Trimethoxybenzoyl)-4,5-dihydro-5-(2,4-dimethoxyphenyl)-3-(3,4-dimethoxyphenyl)-1H-pyrazole (6c)

The residue was chromatographed with ethyl acetate/*n*-hexane (1:4) as eluent to give **6c** as a yellow crystals in (0.43 g, 80.13% yield), mp 105°C. IR (KBr) ν_{\max} (cm⁻¹): 1615 (C=O) and 1585 (C=O). ¹H NMR (300 MHz, CDCl₃) δ (ppm): 3.11 (dd, 1H, *J* = 17.40 and 4.80 Hz, CH₂ of pyrazoline), 3.68–3.74 (m, 1H, CH₂ of pyrazoline), 3.79 (s, 3H, CH₃), 3.80 (s, 3H, CH₃), 3.88 (s, 3H, CH₃), 3.93 (s, 3H, CH₃), 3.94 (s, 3H, CH₃), 3.95 (s, 6H, 2CH₃), 5.98–6.03 (m, 1H, CH of pyrazoline), 6.45 (dd, 1H, *J* = 8.40 and 2.40 Hz, Ar-H), 6.51 (s, 1H, Ar-H), 6.89 (d, 1H, *J* = 8.40 Hz, Ar-H), 7.10 (d, 1H, *J* = 8.40 Hz, Ar-H), 7.19 (dd, 1H, *J* = 8.40 and 1.80 Hz, Ar-H), 7.41 (s, 1H, Ar-H), 7.53 (s, 2H, Ar-H). ¹³C NMR (75 MHz, CDCl₃) δ (ppm):

42.65 (CH₂), 57.37 (CH₃), 57.55 (CH₃), 57.86 (CH₃), 57.98 (CH₃), 58.17 (2CH₃), 59.29 (CH₃), 62.83 (CH), 100.56 (CH), 105.69 (CH), 109.90 (CH), 112.06 (CH), 121.81 (CH), 123.05 (CH), 125.78 (CH), 127.93 (C), 130.50 (C), 141.41 (C), 150.01 (C), 151.97 (C), 153.11 (C), 156.41 (C), 157.97 (C), 161.07 (C), 165.36 (CO). MS (ESI): 537.3 (C₂₉H₃₃N₂O₈, [M+H]⁺). Anal. Calcd. for C₂₉H₃₂N₂O₈: C, 64.91; H, 6.01; N, 5.22. Found: C, 64.66; H, 5.97; N, 5.12.

1-(3,4,5-Trimethoxybenzoyl)-4,5-dihydro-5-(4-methoxyphenyl)-3-(3,4-dimethoxyphenyl)-1H-pyrazole (6d)

The residue was chromatographed with ethyl acetate/*n*-hexane (1:3) as eluent to give **6d** as a yellow powder in (0.41 g, 80.93% yield), mp 93–94°C. IR (KBr) ν_{\max} (cm⁻¹): 1612 (C=N) and 1583 (C=O). ¹H NMR (300 MHz, CDCl₃) δ (ppm): 3.23 (dd, 1H, *J* = 17.40 and 5.20 Hz, CH₂ of pyrazoline), 3.70–3.74 (m, 1H, CH₂ of pyrazoline), 3.81 (s, 3H, CH₃), 3.90 (s, 3H, CH₃), 3.94 (s, 6H, 2CH₃), 3.95 (s, 6H, 2CH₃), 5.76–5.81 (m, 1H, CH of pyrazoline), 6.85–6.91 (m, 3H, Ar-H), 7.17–7.22 (m, 1H, Ar-H), 7.21–7.28 (m, 2H, Ar-H), 7.44 (s, 1H, Ar-H), and 7.49 (s, 2H, Ar-H). ¹³C NMR (75 MHz, CDCl₃) δ (ppm): 43.53 (CH₂), 57.29 (CH₃), 57.87 (CH₃), 58.01 (CH₃), 58.18 (CH₃), 60.36 (CH₃), 62.84 (CH₃), 63.19 (CH), 109.52 (CH), 109.90 (CH), 112.10 (CH), 115.59 (CH), 121.91 (CH), 125.45 (CH), 128.16 (C), 130.21 (C), 135.19 (C), 141.51 (C), 150.01 (C), 152.15 (C), 153.11 (C), 155.74 (C), 159.80 (C), 165.53 (CO). MS (ESI): 507.3 (C₂₈H₃₁N₂O₇, [M+H]⁺). Anal. Calcd. for C₂₈H₃₀N₂O₇: C, 66.39; H, 5.97; N, 5.53. Found: C, 66.25; H, 6.23; N, 5.25.

5-(4-Cyanophenyl)-4,5-dihydro-1-(3,4,5-trimethoxybenzoyl)-3-(3,4-dimethoxyphenyl)-1H-pyrazole (6e)

The residue was chromatographed with ethyl acetate/*n*-hexane (1:3) as eluent to give **6e** as a white powder in (0.41 g, 81.74% yield), mp 188–189°C. IR (KBr) ν_{\max} (cm⁻¹): 2240 (CN), 1610 (C=N), 1578 (C=O). ¹H NMR (300 MHz, CDCl₃) δ (ppm): 3.18 (dd, 1H, *J* = 17.70 and 5.10 Hz, CH₂ of pyrazoline), 3.82–3.89 (m, 1H, CH₂ of pyrazoline), 3.94 (s, 3H, CH₃), 3.95 (s, 6H, 2CH₃), 3.96 (s, 6H, 2CH₃), 5.85 (dd, 1H, *J* = 5.10 and 11.70 Hz, CH of pyrazoline), 6.91 (d, 1H, *J* = 8.10 Hz, Ar-H), 7.19 (dd, 1H, *J* = 8.1, 1.8 Hz, Ar-H), 7.41–7.48 (m, 3H, Ar-H), 7.51 (s, 2H, Ar-H), 7.65–7.68 (m, 2H, Ar-H). ¹³C NMR (75 MHz, CDCl₃) δ (ppm): 43.20 (CH₂), 57.88 (CH₃), 58.04 (CH₃), 58.21 (2CH₃), 62.87 (CH₃), 63.43 (CH), 109.55 (CH), 109.87 (CH), 112.15 (CH), 112.96 (CH), 119.80 (CN), 122.02 (CH), 124.87 (CH), 127.73 (C), 129.42 (C), 133.95 (C), 141.89 (C), 147.95 (C), 150.20 (C), 152.45 (C), 153.21 (C), 155.52 (C), 165.59 (CO). MS (ESI): 502.3 (C₂₈H₂₈N₃O₆, [M+H]⁺). Anal. Calcd. for C₂₈H₂₇N₃O₆: C, 67.05; H, 5.43; N, 8.38. Found: C, 66.91; H, 5.59; N, 8.37.

5-(3-Hydroxyphenyl)-4,5-dihydro-1-(3,4,5-trimethoxybenzoyl)-3-(3,4-dimethoxyphenyl)-1H-pyrazole (6f)

The residue was chromatographed with ethyl acetate/*n*-hexane (1:2) as eluent to give **6f** as a white powder in (0.40 g, 81.30% yield), mp 118–119°C. IR (KBr) ν_{\max} (cm⁻¹): 3250 (OH), 1609 (C=N), and 1570 (C=O). ¹H NMR (300 MHz, CDCl₃) δ (ppm): 3.14 (dd, 1H, *J* = 17.40 and 4.50 Hz, CH₂ of pyrazoline), 3.77–3.80 (m, 1H, CH₂ of pyrazoline), 3.81 (s, 3H, CH₃), 3.82 (s, 3H, CH₃), 3.84 (s, 3H, CH₃), 3.87 (s, 6H, 2CH₃), 5.66 (dd, 1H, *J* = 4.50 and 11.70 Hz, CH of pyrazoline), 6.63–6.71 (m, 3H, Ar-H), 6.93 (d, 1H, *J* = 8.40 Hz, Ar-H), 7.09 (t, 1H, *J* = 7.8 Hz, Ar-H), 7.21 (dd, 1H, *J* = 7.8, 2.10 Hz, Ar-H), 7.32 (d, 1H, *J* = 1.80 Hz, Ar-H), 7.41 (s, 2H, Ar-H), 8.04 (s, 1H, OH). ¹³C NMR (75 MHz, CDCl₃)

δ (ppm): 43.51 (CH₂), 62.42 (CH₃), 62.67 (CH₃), 62.93 (2 CH₃), 67.21 (CH₃), 68.06 (CH), 114.22 (CH), 115.18 (CH), 115.23 (CH), 117.56 (CH), 118.44 (CH), 120.63 (CH), 122.26 (CH), 126.80 (CH), 130.04 (C), 135.22 (C), 135.72 (C), 146.06 (C), 149.68 (C), 154.76 (C), 156.86 (C), 157.85 (C), 160.90 (C), 163.52 (C), 169.46 (CO). MS (ESI): 493.3 (C₂₇H₂₉N₂O₇, [M+H]⁺). Anal. Calcd. for C₂₇H₂₈N₂O₇: C, 65.84; H, 5.73; N, 5.69. Found: C, 65.55; H, 5.82; N, 5.57.

5-(3-Hydroxyphenyl)-4,5-dihydro-1-(3,4,5-trimethoxybenzoyl)-3-(4-methoxyphenyl)-1H-pyrazole (**6g**)

The residue was chromatographed with ethyl acetate/*n*-hexane (1:2) as eluent to give **6g** as a white powder in (0.37 g, 89% yield), mp 189–191°C. IR (KBr) ν_{\max} (cm⁻¹): 3380 (OH), 1610 (C=N), and 1580 (C=O). ¹H NMR (300 MHz, CDCl₃) δ (ppm): 3.14 (dd, 1H, *J* = 17.40 and 4.50 Hz, CH₂ of pyrazoline), 3.71 (dd, 1H, *J* = 17.40 and 11.40 Hz, CH₂ of pyrazoline), 3.86 (s, 3H, CH₃), 3.91 (s, 3H, CH₃), 3.95 (s, 6H, 2CH₃), 5.70 (dd, 1H, *J* = 4.50 and 11.40 Hz, CH of pyrazoline), 6.66 (dd, 1H, *J* = 7.80 and 1.50 Hz, Ar-H), 6.76–6.80 (m, 2H, Ar-H), 6.93 (d, 2H, *J* = 8.7 Hz, Ar-H), 7.12 (t, 1H, *J* = 7.8 Hz, Ar-H), 7.48 (s, 2H, Ar-H), 7.67 (d, 2H, *J* = 8.7 Hz, Ar-H), 8.10 (s, 1H, OH). ¹³C NMR (75 MHz, CDCl₃) δ (ppm): 43.73 (CH₂), 57.43 (CH₃), 58.23 (CH₃), 62.42 (CH₃), 62.84 (CH₃), 63.64 (CH), 109.56 (CH), 114.47 (CH), 115.55 (CH), 116.33 (CH), 117.54 (CH), 124.92 (CH), 129.51 (CH), 129.92 (C), 131.27 (C), 141.62 (C), 143.98 (C), 153.15 (C), 156.68 (C), 157.82 (C), 162.32 (C), 166.20 (CO). MS (ESI): 463.3 (C₂₆H₂₇N₂O₆, [M+H]⁺). Anal. Calcd. for C₂₆H₂₆N₂O₆: C, 67.52; H, 5.67; N, 6.06. Found: C, 67.42; H, 5.87; N, 6.01.

Biological evaluation

Anticancer activity

The methodology of the NCI anticancer screening has been described in detail elsewhere (<http://www.dtp.nci.nih.gov>). Briefly, the primary anticancer assay was performed at approximately 60 human tumor cell lines panel derived from nine neoplastic diseases, in accordance with the protocol of the Drug Evaluation Branch, National Cancer Institute, Bethesda. Tested compounds were added to the culture at a single concentration (10⁻⁵ M) and the cultures were incubated for 48 h. End point determinations were made with a protein binding dye, SRB. Results for each tested compound were reported as the percent of growth of the treated cells when compared to the untreated control cells. The percentage growth was evaluated spectrophotometrically versus controls not treated with test agents. The cytotoxic and/or growth inhibitory effects of the most active selected compound were tested *in vitro* against the full panel of about 60 human tumor cell lines at 10-fold dilutions of five concentrations ranging from 10⁻⁴ to 10⁻⁸ M. A 48-h continuous drug exposure protocol was followed and an SRB protein assay was used to estimate cell viability or growth. Using the seven absorbance measurements [time zero (*T*_z), control growth in the absence of drug (*C*), and test growth in the presence of drug at the five concentration levels (*T*_i)], the percentage growth was calculated at each of the drug concentrations levels. Percentage growth inhibition was calculated as: $[(T_i - T_z)/(C - T_z)] \times 100$ for concentrations for which *T*_i > *T*_z, and $[(T_i - T_z)/T_z] \times 100$ for concentrations for which *T*_i < *T*_z. Three dose-response parameters were calculated for each compound. Growth inhibition of 50% (GI₅₀) was calculated from $[(T_i - T_z)/(C - T_z)] \times 100 = 50$, which is the drug concentration resulting in a 50% lower net protein increase in the

treated cells (measured by SRB staining) as compared to the net protein increase seen in the control cells. The drug concentration resulting in TGI was calculated from *T*_i = *T*_z. The LC₅₀ (concentration of drug resulting in a 50% reduction in the measured protein at the end of the drug treatment as compared to that at the beginning) indicating a net loss of cells following treatment was calculated from $[(T_i - T_z)/T_z] \times 100 = -50$. Values were calculated for each of these three parameters if the level of activity is reached; however, if the effect was not reached or was exceeded, the value for that parameter was expressed as more or less than the maximum or minimum concentration tested. The log GI₅₀, log TGI, and log LC₅₀ were then determined, defined as the mean of the logs of the individual GI₅₀, TGI, and LC₅₀ values. The lowest values are obtained with the most sensitive cell lines. Compound having logGI₅₀ values -4 and <-4 was declared to be active.

Assay of microtubule assembly

Solubility of the tested compounds

A stock solution of each compound was prepared in DMSO. Each compound stock was diluted in PME buffer {100 mM PIPES, 1 mM MgSO₄, 2 mM ethylene glycol bis[β-aminoethyl ether]N,N'-tetraacetic acid (EGTA), pH 6.90 at 25°C} to yield concentrations up to 80 μM and a final DMSO concentration of 2–8%. Samples of identical concentrations were also prepared in 100% DMSO. Absorbance spectra of these samples were obtained using a HP 8453 UV-Vis spectrophotometer. The compound's aqueous solubility was assessed by the overlaid absorbance spectra of the 2–8% and 100% DMSO samples for the same concentration. Significant changes in light scattering of the 2–8% DMSO sample compared to the 100% DMSO sample suggested insolubility of the compound under experimental conditions.

Screening for tubulin polymerization inhibition [60]

DMSO or 40 μM of the ligand in DMSO was added to bovine brain tubulin (final concentration of 5 μM) in PME buffer and incubated for 40 min at room temperature in a 96-well plate. GTP and DAPI were added to obtain final concentrations of 0.1 mM and 10 μM, respectively. The samples were equilibrated to 37°C in the SynergyMx microplate reader for 5 min and the fluorescence was recorded to establish a baseline. The excitation and emission wavelengths were 360 and 450 nm, respectively. Paclitaxel in DMSO was added to a final concentration of 5 μM to induce microtubule assembly. The total concentration of DMSO was limited to 4% v/v; ligand and paclitaxel were each added in 2% DMSO of the final volume. The extent of polymerization was monitored over time by an increase in fluorescence at 450 nm.

IC₅₀ determination

Bovine brain tubulin (8 μM), GTP (1 mM), and DAPI (10 μM) in PME buffer were equilibrated to 37°C in the 96-well plates. The excitation and emission wavelengths were set at 360 and 450 nm, respectively, and the fluorescence was recorded to obtain a baseline. Varying concentration of the ligand in DMSO was added and the increase in fluorescence was monitored over time. The control contained tubulin, GTP, DAPI, and DMSO but no ligand. The final concentration of DMSO was 8% v/v in all

samples. The extent of polymerization versus the log of ligand concentration was plotted, and the IC₅₀ value was calculated from the sigmoidal fit of the dose–response curve.

Confocal microscopy

PC3 cells were grown on Lab-Tek II chambered cover glass slips for 24 h and then treated with 1% DMSO or 20 μM ligand in 1% DMSO for 24 h. Cells were washed three times with PBS (10 mM sodium phosphate, pH 7.2, 0.9% sodium chloride w/v) and then treated with methanol/acetone (1:1 v/v) for 10 min at 4°C. The cells were washed again three times with PBS and incubated with 5% bovine serum albumin (BSA) in PBST (PBS with 0.1% Tween) for 30 min. The cells were then incubated with mouse monoclonal anti-α tubulin antibody (Zymed Technologies) for 1 h and with Alexafluor 647 goat anti-mouse IgG (Molecular probes) for 45 min at room temperature. The nucleus was stained with DAPI (0.1 μg/mL) and Gel/Mount (Biomedica Corp.) was added before imaging. In between each step, the cells were washed with PBS thrice. Photomicrographs were obtained using a Zeiss LSM 510 META confocal scanning laser microscope.

Molecular docking

All the molecular modeling studies were carried out on an Intel Core™ i3 processor, 3 GB memory with Windows 7 operating system using Molecular Operating Environment (MOE 2008, Chemical Computing Group, Canada) as the computational software. All the minimizations were performed with MOE until a RMSD gradient of 0.05 kcal mol⁻¹ Å⁻¹ with MMFF94X force-field and the partial charges were automatically calculated.

The X-ray crystallographic structure of tubulin complexed with DAMA–colchicine (PDB ID: 1SA0) was obtained from the protein data bank. The enzyme was prepared for docking studies where: (i) Ligand molecule was removed from the enzyme active site. (ii) Hydrogen atoms were added to the structure with their standard geometry. (iii) MOE Alpha Site Finder was used for the active sites search in the enzyme structure and dummy atoms were created from the obtained alpha spheres. (iv) The obtained model was then used in predicting the ligand–enzyme interactions at the active site.

Authors thank the Development Therapeutics Program of the National Cancer Institute, Bethesda, MD, USA, for *in vitro* evaluation of anticancer activity.

The authors have declared no conflict of interest.

References

- [1] M. Harrison, K. Hohen, G. Liu, *Clin. Adv. Hematol. Oncol.* **2009**, *7*, 54–64.
- [2] P. A. Gehrig, V. L. Bae-Jump, *Gynecol. Oncol.* **2010**, *116*, 187–194.
- [3] G. R. Pettit, S. B. Singh, E. Hamel, C. M. Lin, D. S. Alberts, D. Garcia-Kendall, *Experientia* **1989**, *45*, 209–211.
- [4] J. A. Woods, J. A. Hadfield, G. R. Pettit, B. W. Fox, A. T. McGown, *Br. J. Cancer* **1995**, *71*, 705–711.
- [5] E. K. Rowinsky, R. C. Donehower, *Pharmacol. Ther.* **1991**, *52*, 35–84.
- [6] K. Odlo, J. Hentzen, J. F. dit Chabert, S. Ducki, O. Gani, I. Sylte, M. Skrede, V. A. Florenes, T. V. Hansen, *Bioorg. Med. Chem.* **2008**, *16*, 4829–4838.
- [7] D. Simoni, R. Romagnoli, R. Baruchello, R. Rondanin, G. Grisolia, M. Eleopra, M. Rizzi, M. Tolomeo, G. Giannini, D. Alloatti, M. Castorina, M. Marcellini, *J. Med. Chem.* **2008**, *51*, 6211–6215.
- [8] D. Simoni, R. Romagnoli, R. Baruchello, R. Rondanin, M. Rizzi, M. G. Pavani, D. Alloatti, G. Giannini, M. Marcellini, T. Riccioni, M. Castorina, M. B. Guglielmi, F. Bucci, P. Carminati, C. Pisano, *J. Med. Chem.* **2006**, *49*, 3143–3152.
- [9] G. C. Tron, T. Pirali, G. Sorba, F. Pagliai, S. Bussacca, A. A. Genazzani, *J. Med. Chem.* **2006**, *49*, 3033–3044.
- [10] Q. Zhang, Y. Peng, X. I. Wang, S. M. Keenan, S. Arora, W. J. Welsh, *J. Med. Chem.* **2007**, *50*, 749–754.
- [11] J. P. Liou, Y. L. Chang, F. M. Kuo, C. W. Chang, H. Y. Tseng, C. C. Wang, Y. N. Yang, J. Y. Chang, S. J. Lee, H. P. Hsieh, *J. Med. Chem.* **2004**, *47*, 4247–4257.
- [12] G. De Martino, M. C. Edler, G. La Regina, A. Coluccia, M. C. Barbera, D. Barrow, R. I. Nicholson, G. Chiosis, A. Brancale, E. Hamel, M. Artico, R. Silvestri, *J. Med. Chem.* **2006**, *49*, 947–954.
- [13] J. X. Duan, X. Cai, F. Meng, L. Lan, C. Hart, M. Matteucci, *J. Med. Chem.* **2007**, *50*, 1001–1006.
- [14] N. H. Nam, *Curr. Med. Chem.* **2003**, *10*, 1697–1722.
- [15] L. Sun, N. I. Vasilevich, J. A. Fuselier, S. J. Hocart, D. H. Coy, *Bioorg. Med. Chem. Lett.* **2004**, *14*, 2041–2046.
- [16] H. P. Hsieh, J. P. Liou, N. Mahindroo, *Curr. Pharm. Des.* **2005**, *11*, 1655–1677.
- [17] D. J. Chaplin, G. J. Dougherty, *Br. J. Cancer* **1999**, *80*, 57–64.
- [18] G. M. Tozer, C. Kanthou, C. S. Parkins, S. A. Hill, *Int. J. Exp. Pathol.* **2002**, *83*, 21–38.
- [19] C. Kanthou, G. M. Tozer, *Exp. Opin. Ther. Targets* **2007**, *11*, 1443–1457.
- [20] D. W. Siemann, D. J. Chaplin, P. A. Walicke, *Exp. Opin. Invest. Drugs* **2009**, *18*, 189–197.
- [21] R. LeBlanc, J. Dickson, T. Brown, M. Stewart, H. N. Pati, D. VanDerveer, H. Arman, J. Harris, W. Pennington, H. L. Holt, Jr M. Lee, *Bioorg. Med. Chem.* **2005**, *13*, 6025–6034.
- [22] C. M. Lin, S. B. Singh, P. S. Chu, R. O. Dempcy, J. M. Schmidt, G. R. Pettit, E. Hamel, *Mol. Pharmacol.* **1988**, *34*, 200–208.
- [23] K. Ohsumi, T. Hatanaka, K. Fujita, R. Nakagawa, Y. Fukuda, Y. Nihei, Y. Suga, Y. Morinaga, Y. Akiyama, T. Tsuji, *Bioorg. Med. Chem. Lett.* **1998**, *8*, 3153–3158.
- [24] L. Wang, K. W. Woods, Q. Li, K. J. Barr, R. W. McCroskey, S. M. Hannick, L. Gherke, R. B. Credo, Y. H. Hui, K. Marsh, R. Warner, J. Y. Lee, N. Zielinski-Mozng, D. Frost, S. H. Rosenberg, H. L. Sham, *J. Med. Chem.* **2002**, *45*, 1697–1711.
- [25] G. R. Pettit, M. R. Rhodes, D. L. Herald, E. Hamel, J. M. Schmidt, R. K. Pettit, *J. Med. Chem.* **2005**, *48*, 4087–4099.
- [26] G. R. Pettit, M. P. Grealish, D. L. Herald, M. R. Boyd, E. Hamel, R. K. Pettit, *J. Med. Chem.* **2000**, *43*, 2731–2737.
- [27] M. Medarde, A. C. Ramos, E. Caballero, R. Pelaez-Lamamie de Clairac, J. L. Lopez, D. G. Gravalos, A. S. Feliciano, *Bioorg. Med. Chem. Lett.* **1999**, *9*, 2303–2308.
- [28] N. H. Nam, Y. Kim, Y. J. You, D. H. Hong, H. M. Kim, B. Z. Ahn, *Bioorg. Med. Chem. Lett.* **2001**, *11*, 1173–1176.

- [29] N. H. Nam, Y. Kim, Y. J. You, D. H. Hong, H. M. Kim, B. Z. Ahn, *Bioorg. Med. Chem. Lett.* **2002**, 12, 1955–1958.
- [30] C. C. Kuo, H. P. Hsieh, W. Y. Pan, C. P. Chen, J. P. Liou, S. J. Lee, Y. L. Chang, L. T. Chen, C. T. Chen, J. Y. Chang, *Cancer Res.* **2004**, 64, 4621–4628.
- [31] C. Borrel, S. Thoret, X. Cachet, D. Guenard, F. Tillequin, M. Koch, S. Michel, *Bioorg. Med. Chem.* **2005**, 13, 3853–3864.
- [32] X. Ouyang, E. L. Piatnitski, V. Pattaropong, X. Chen, H. Y. He, A. S. Kiselyov, A. Velankar, J. Kawakami, M. Labelle, L. Smith, II J. Lohman, S. P. Lee, A. Malikzay, J. Fleming, J. Gerlak, Y. Wang, R. L. Rosler, K. Zhou, S. Mitelman, M. Camara, D. Surguladze, J. F. Doody, M. C. Tuma, *Bioorg. Med. Chem. Lett.* **2006**, 16, 1191–1196.
- [33] G. R. Pettit, B. Toki, D. L. Herald, P. Verdier-Pinard, M. R. Boyd, E. Hamel, R. K. Pettit, *J. Med. Chem.* **1998**, 41, 1688–1695.
- [34] J. P. Liou, C. W. Chang, J. S. Song, Y. N. Yang, C. F. Yeh, H. Y. Tseng, Y. K. Lo, Y. L. Chang, C. M. Chang, H. P. Hsieh, *J. Med. Chem.* **2002**, 45, 2556–2562.
- [35] R. Romagnoli, P. G. Baraldi, T. Sarkar, M. D. Carrion, O. Cruz-Lopez, C. Lopez-Cara, M. Tolomeo, S. Grimaudo, A. Di Cristina, M. R. Pipitone, J. Balzarini, R. Gambari, L. Ilaria, R. Saletti, A. Brancale, E. Hamel, *Bioorg. Med. Chem.* **2008**, 16, 8419–8426.
- [36] K. G. Pinney, A. D. Bounds, K. M. Dingerman, V. P. Mocharla, G. R. Pettit, R. Bai, E. Hamel, *Bioorg. Med. Chem. Lett.* **1999**, 9, 1081–1086.
- [37] R. Romagnoli, P. G. Baraldi, M. D. Carrion, C. L. Cara, O. Cruz-Lopez, D. Preti, M. Tolomeo, S. Grimaudo, A. Di Cristina, N. Zonta, J. Balzarini, A. Brancale, T. Sarkar, E. Hamel, *Bioorg. Med. Chem.* **2008**, 16, 5367–5376.
- [38] R. Romagnoli, P. G. Baraldi, O. Cruz-Lopez, M. Tolomeo, A. Di Cristina, R. M. Pipitone, S. Grimaudo, J. Balzarini, A. Brancale, E. Hamel, *Bioorg. Med. Chem. Lett.* **2011**, 21, 2746–2751.
- [39] R. Romagnoli, P. G. Baraldi, T. Sarkar, M. D. Carrion, C. Lopez-Cara, O. Cruz-Lopez, D. Preti, M. A. Tabrizi, M. Tolomeo, S. Grimaudo, A. Di Cristina, N. Zonta, J. Balzarini, A. Brancale, H. P. Hsieh, E. Hamel, *J. Med. Chem.* **2008**, 51, 1464–1468.
- [40] A. K. Tewari, A. Mishra, *Bioorg. Med. Chem.* **2001**, 9, 715–718.
- [41] R. H. Wiley, P. Wiley, *Pyrazolones, Pyrazolidones and Derivatives*, John Wiley and Sons, New York **1964**.
- [42] S. Bondock, W. Khalifa, A. A. Fadda, *Eur. J. Med. Chem.* **2011**, 46, 2555–2561.
- [43] S. L. Janus, A. Z. Magdif, B. P. Erik, N. Claus, *Monatsh. Chem.* **1999**, 130, 1167–1174.
- [44] H. J. Park, K. Lee, S. J. Park, B. Ahn, J. C. Lee, H. Cho, K. I. Lee, *Bioorg. Med. Chem. Lett.* **2005**, 15, 3307–3312.
- [45] V. Michon, C. H. Du Penhoat, F. Tombret, J. M. Gillardin, F. Lepage, L. Berthon, *Eur. J. Med. Chem.* **1995**, 30, 147–155.
- [46] I. Yildirim, N. Ozdemir, Y. Akçamur, M. Dinçer, O. Andaç, *Acta Crystallogr.* **2005**, E61, o256–o258
- [47] D. M. Bailey, P. E. Hansen, A. G. Hlavac, E. R. Baizman, J. Pearl, A. F. DeFelice, M. E. Feigenson, *J. Med. Chem.* **1985**, 28, 256–260.
- [48] M. Abdel-Aziz, A. M. Gamal-Eldeen, *Pharm. Biol.* **2009**, 47, 854–863.
- [49] M. E. Shoman, M. Abdel-Aziz, O. M. Aly, H. H. Farag, M. A. Morsy, *Eur. J. Med. Chem.* **2009**, 44, 3068–3076.
- [50] el-S. M. M. N. Abdel-Hafez, Gel-D. A. A. Abu-Rahma, M. Abdel-Aziz, M. F. Radwan, H. H. Farag, *Bioorg. Med. Chem.* **2009**, 17, 3829–3837.
- [51] N. Mahindroo, J. P. Liou, J. Y. Chang, H. P. Hsieh, *Expert Opin. Ther. Pat.* **2006**, 16, 647–691.
- [52] M. A. Jordan, L. Wilson, *Nat. Rev. Cancer* **2004**, 4, 253–265.
- [53] A. Chaudhary, S. N. Pandeya, P. Kumar, P. P. Sharma, S. Gupta, N. Soni, K. K. Verma, G. Bhardwaj, *Mini-Rev. Med. Chem.* **2007**, 7, 1186–1205.
- [54] H. P. Hsieh, J. P. Liou, N. Mahindroo, *Curr. Pharm. Des.* **2005**, 11, 1655–1677.
- [55] E. M. Acton, V. L. Narayanan, P. A. Risbood, R. H. Shoemaker, D. T. Vistica, M. R. Boyd, *J. Med. Chem.* **1994**, 37, 2185–2189.
- [56] C. E. Kung, J. K. Reed, *Biochemistry* **1989**, 28, 6678–6686.
- [57] D. Bonne, C. Heusele, C. Simon, D. Pantaloni, *J. Biol. Chem.* **1985**, 260, 2819–2825.
- [58] S. Desbène, S. Giorgi-Renault, *Curr. Med. Chem. Anticancer Agents* **2002**, 2, 71–90.
- [59] B. A. Bhat, K. L. Dhar, S. C. Puri, A. K. Saxena, M. Shanmugavel, G. N. Qazi, *Bioorg. Med. Chem. Lett.* **2005**, 15, 3177–3180.
- [60] D. M. Barron, S. K. Chatterjee, R. Ravindra, R. Roof, E. Baloglu, D. G. Kingston, S. Bane, *Anal. Biochem.* **2003**, 315, 49–56.